



Ion induced promotion of activity enhancement of mesoporous manganese oxides for aerobic oxidation reactions

Sourav Biswas, Altug S. Poyraz, Yongtao Meng, Chung-Hao Kuo, Curtis Guild, Hannah Tripp, Steven L. Suib*

Department of Chemistry and Institute of Materials Science, University of Connecticut, 55 North Eagleville Road, U-3060, Storrs, CT 06269, United States

ARTICLE INFO

Article history:

Received 29 May 2014

Received in revised form 17 October 2014

Accepted 21 October 2014

Available online 1 November 2014

Keywords:

Mesoporous

Manganese oxide

Cation promoted

Alcohol oxidation

Lattice oxygen

ABSTRACT

Inverse micelle templated mesoporous manganese oxide (University of Connecticut mesoporous material, UCT-1) and ion promoted mesoporous manganese oxides (UCT-18-X, X = Mg^{2+} , Ca^{2+} , K^+ , Na^+ and Cs^+) having trace amount of alkali metal ions as promoters with tunable porosity and crystallinity were synthesized. The synthesis was based on the use of inverse micelles as soft templates and unique NO_x chemistry as established for recently discovered UCT materials. The materials were tested for selective aerobic alcohol oxidation and the catalytic activity followed the order of $\text{UCT-1} < \text{UCT-18-Mg} < \text{UCT-18-Ca} < \text{UCT-18-K} < \text{UCT-18-Na} < \text{UCT-18-Cs}$. The catalytic activity was correlated to the promoter ion induced increase in basicity of the materials. The retention of an amorphous structure, low reducibility, and the effects of lattice oxygen are other key factors responsible for the enhanced catalytic activity. The UCT-18-Cs catalyst was found to oxidize various alcohols to corresponding aldehydes and ketones selectively (100% selectivity) with very high conversion (as high as 100%). The UCT-18-Cs also exhibited solvent free green oxidation of 1,3,5-trimethylbenzene to yield 3,5-dimethylbenzoic acid and (3,5-dimethylphenyl)methyl ester with >90% conversion and 90% selectivity for the acid and 9% selectivity for the ester.

© 2014 Published by Elsevier B.V.

1. Introduction

Since the discovery of mesoporous silica and aluminosilicates (M41S family) by Mobil Oil Corporation in 1992 [1] mesoporous materials have attracted a great deal of interest in the field of heterogeneous catalysis in organic transformations [2,3]. Specifically, mesoporous transition metal oxides (MTMO) have shown promise for performing a wide range of catalytic organic transformations due to the co-existence of multiple oxidation states [4]. Transition metal oxides can be further modified with several dopants and promoter ions to design a specific catalyst for specific reactions [5–8]. Among the transition metal oxides, manganese oxides deserve a special interest, since manganese can exist in more than five stable and easily exchangeable oxidation states with multiple structural forms over a wide range of temperatures. Manganese oxides have a wide range of catalytic applications due to highly efficient redox properties [9–11], and can be more effective in the presence of other elements [12]. Manganese oxides are also known to be effective oxidation catalysts in both the amorphous and crystalline states

[13–17]. Like other transition metal oxides, manganese oxides can also accommodate cations either on the surface as promoter ions [18] or in their structures as charge balancing ions [19] (as in octahedral molecular sieve, $\text{KMn}_8\text{O}_{16} \cdot n\text{H}_2\text{O}$ or K-OMS-2, where K^+ resides in the tunnel for charge balancing).

Liquid phase oxidation reactions are of interest in organic chemistry as well as in industrial applications. The selective oxidation of alcohols to carbonyl compounds is one of the common and elegant classes of molecular transformations in synthetic organic chemistry. The desired carbonyl products are high value components used in fine chemicals, pharmaceutical, and perfume industries [20]. Numerous catalytic systems have been used to perform this partial oxidation of alcohols [21–23]. The two major problems associated with heterogeneous catalysts are the lifetime of the catalyst (catalyst deactivation) and the leaching of active species from the solid surface to the solution [24]. The design of an efficient heterogeneous catalyst system should ideally involve mild and environmentally friendly reaction conditions (air as the oxidant, low temperature, low catalyst loading, avoidance of toxic materials, and minimum waste disposal with proper reusability) in addition to high efficiency. The selective C–H bond oxidation at the benzylic position to the corresponding oxy functional products is an important and challenging aspect in synthetic organic chemistry

* Corresponding author. Tel.: +1 860 486 2797; fax: +1 860 486 2981.
E-mail address: steven.suib@uconn.edu (S.L. Suib).

[25–28]. For example, the methyl benzoic acids (oxidation products of methyl aromatics) have versatile use in chemical and pharmaceutical industries [29]. Traditionally, stoichiometric amounts of oxidants like potassium permanganate (KMnO_4), chromium trioxide (CrO_3), sodium dichromate ($\text{Na}_2\text{Cr}_2\text{O}_7$) and nitric acid (HNO_3) [30] are required in these oxidation reactions. The production of large amounts of toxic wastes and the requirement of difficult separation steps make these processes environmentally and industrially unfavorable. Despite the industrial importance, environmentally friendly oxidation processes are rarely described in the literature. Some efficient catalytic systems involve oxidants such as metaloxo materials, *tert*-butyl hydroperoxide (TBHP) or hydrogen peroxide (H_2O_2) and base additives [31–34]. However, these systems often suffer from low conversion (of alkylbenzenes) and require the use of conditions like high pressure and temperature. An efficient and economically feasible catalyst system should perform alkylbenzene oxidation with high selectivity towards the corresponding acid under aerobic condition.

Recently synthesized UCT (University of Connecticut) mesoporous materials form quite a large family [35]. The UCT synthetic approach allows one to synthesize different mesoporous oxide materials using a single synthetic strategy, i.e. transition metals, metalloids, mixed oxides and promoted oxides [36]. The synthesis relies on inverse micelle formation and unique NO_x chemistry. The NO_x species are formed in situ by thermal decomposition of NO_3^- . The metal oxide nanoparticles are packed closely in a random fashion to build the mesostructure. The UCT materials were found to be active in different types of catalytic reactions. For example, Cs promoted mesoporous manganese oxide (UCT-18-Cs) exhibited a bifunctional catalytic role (oxidation and then in situ esterification). The inactivated aliphatic alcohol 1-decanol was oxidized to 1-decanoic acid and then 1-decanoic acid combined with 1-decanol to produce decyl decanoate. Whereas, nonpromoted UCT-1 and other manganese oxide catalysts (K-OMS-2, amorphous manganese oxide, Mn_2O_3) could only perform oxidation of 1-decanol to 1-decanal. The oxidation of inactivated long chain alcohol demonstrates the redox power of the catalyst, while the esterification is due to the basic nature of the catalyst. In this work 5 different UCT-18 materials were synthesized using 5 different promoter cations (Mg^{2+} , Ca^{2+} , K^+ , Na^+ and Cs^+) with tunable mesostructure parameters (such as pore size, pore volume, surface area). Selective aerobic oxidations of alcohols and oxidations of inert alkylbenzenes were performed using the catalysts and the catalytic activity was also compared with conventional active manganese oxide catalysts.

2. Experimental section

2.1. Catalyst synthesis

2.1.1. Synthesis of UCT-1

In a typical synthesis 0.02 mol of manganese nitrate tetrahydrate ($\text{Mn}(\text{NO}_3)_2 \cdot 4\text{H}_2\text{O}$) and 0.134 mol of 1-Butanol were added into a 120 mL beaker. To this solution 0.0034 mol of Poly(ethylene glycol)-*block*-poly(propylene glycol)-*block*-poly(ethylene glycol) (Pluoronic P123, $\text{PEO}_{20}\text{PPO}_{70}\text{PEO}_{20}$, molar mass 5750 g mol⁻¹) and 0.032 mol of concentrated nitric acid (HNO_3) were added and stirred at room temperature until the solution became clear (light pink). The solution was then kept in an oven at 120 °C for 3 h under air. The resulting black material was washed with excess ethanol, centrifuged and dried in a vacuum oven overnight. The dried black powders were subjected to a heating cycle. First they were heated at 150 °C for 12 h and cooled down to room temperature under ambient conditions followed by a second heating step of 250 °C for 3 h.

2.1.2. Synthesis of UCT-18

In a typical synthesis 0.02 mol of manganese nitrate tetrahydrate ($\text{Mn}(\text{NO}_3)_2 \cdot 4\text{H}_2\text{O}$) and 0.134 mol of 1-Butanol were added into a 120 mL beaker. To this solution 0.0034 mol of Poly(ethylene glycol)-*block*-poly(propylene glycol)-*block*-poly(ethylene glycol) (Pluoronic P123, $\text{PEO}_{20}\text{PPO}_{70}\text{PEO}_{20}$, molar mass 5750 g mol⁻¹) and 0.032 mol of concentrated nitric acid (HNO_3) were added and stirred at room temperature until the solution became clear (light pink). To this clear solution 200 μL of 1.0 M XNO_3 ($\text{X} = \text{Cs}, \text{K}, \text{Na}$) and $\text{X}(\text{NO}_3)_2$ ($\text{X} = \text{Ca}, \text{Mg}$) was added maintaining the Mn/X ratio 100/1, mol/mol. The resulting clear solution was then kept in an oven at 120 °C for 3 h under air. The black material was washed with excess ethanol, centrifuged, and dried in a vacuum oven overnight. The dried black powders were subjected to a heating cycle. First they were heated at 150 °C for 12 h and cooled down to room temperature under ambient conditions followed by a second heating step of 250 °C for 3 h¹.

2.2. Catalyst characterization

The powder X-Ray diffraction (PXRD) analyses were performed on a Rigaku Ultima IV diffractometer ($\text{Cu K}\alpha$ radiation, $\lambda = 1.5406 \text{ \AA}$) with an operating voltage of 40 kV and a current of 44 mA. The low-angle PXRD patterns were collected over a 2θ range of 0.5–10° with a continuous scan rate of 0.5° min⁻¹, where the wide-angle PXRD patterns were collected over a 2θ range of 5–75° with a continuous scan rate of 1.0° min⁻¹. The Nitrogen adsorption desorption experiments were done with a Quantachrome Autosorb-1-1C automated adsorption system. The samples were degassed at 150 °C for 6 h under helium prior to measurement. The surface areas were calculated using the Brunauer–Emmett–Teller (BET) method and pore sizes and pore volumes were calculated from the desorption branch of the isotherm using the Barrett–Joyner–Halenda (BJH) method. A Zeiss DSM 982 Gemini field emission scanning electron microscope (FE-SEM) with a Schottky emitter at an accelerating voltage of 2.0 kV and a beam current of 1.0 mA was used for determination of surface morphology of the materials. The samples were ultrasonically dispersed in ethanol and deposited on silicon wafers prior to the analyses. High-resolution transmission electron microscopy (HR-TEM) images were recorded on a JEOL 2010 FastEM microscope operating at 200 kV. The samples were prepared by using a focused-ion-beam (FIB) technique to make thin films to be observed by HR-TEM. The CO_2 chemisorption experiments were performed using a Quantachrome Autosorb-1-1C automated adsorption system. All the samples were heated in helium under vacuum at 150 °C for 6 h prior to the experiment. The adsorption studies of UCT-18 and UCT-1 were done at room temperature. Then both adsorption and desorption isotherms were measured for UCT-18-Cs, UCT-1, K-OMS-2 and commercial Mn_2O_3 at 0 °C, 25 °C and –78 °C. Temperature-resolved in situ powder X-ray diffraction (TR-PXRD) analysis was performed in an XTRA X-ray diffractometer ($\text{Cu K}\alpha$ radiation) equipped with an Anton Parr XRK 900 heating chamber. The structural stabilities of UCT-1 and UCT-18 Cs materials were investigated from 250 °C to 550 °C using a ramp rate of 5 °C min⁻¹ under air. Diffraction patterns were obtained in the range of 5–75° 2θ at a scanning rate of 2.0° min⁻¹. X-ray photoelectron spectroscopy (XPS) was done on a PHI model 590 spectrometer with multiprobes (Φ Physical Electronics Industries Inc.), using Al-K radiation ($\lambda = 1486.6 \text{ eV}$) as the radiation source. The powder samples were pressed on carbon tape mounted on adhesive copper tape stuck to a sample stage placed in the analysis chamber. The XPS spectra were analyzed and fitted using CasaXPS software (version

¹ It is recommended to perform all reactions in ovens with proper ventilation due to release of toxic NO_x from the gel during the reaction.

2.3.12). The C 1s photoelectron line at 284.6 eV was used as a reference for correction of the surface charging. A mixture of Gaussian (70%) and Lorentzian (30%) functions was used for the least-squares curve fitting procedure. The temperature programmed reduction (TPR), temperature programmed oxidation (TPO), and mass spectrometry were done with a Thermolyne 79300 model tube furnace equipped with an MKS gas analyzer coupled with a quadrupole mass selective detector. The samples were treated with Ar for 2 h at 250 °C before the experiment. In the experiments 10% vol. H₂ in Ar (for H₂-TPR) and 10% vol. O₂ in Ar (for O₂-TPO) mixtures were used at a constant flow rate in the temperature range 50–600 °C at a ramp of 10 °C min⁻¹. The temperature programmed desorption (TPD) experiments were performed with the same Thermolyne 79300 model tube furnace equipped with an MKS gas analyzer coupled with a quadrupole mass selective detector using pure Ar as carrier gas. The sample was used without any pretreatment. The identification of the products and the conversions of alcohol and mesitylene oxidations were measured by gas chromatography–mass spectrometry (GC–MS) methods using a 7820A GC system connected with a thermal conductivity detector of 5975 series MSD from Agilent Technologies. A nonpolar cross-linked methyl siloxane column with dimensions of 12 in × 0.200 mm × 0.33 μm was used. The atomic adsorption spectroscopy (AAS) was measured by a Varian AA-4 updated atomic absorption spectrometer with a deuterium background corrected hollow cathode lamp, at the respective resonance line using an air-acetylene flame.

2.3. Catalytic activity measurements

2.3.1. Alcohol oxidation

In a typical alcohol oxidation procedure, alcohol (1.0 mmol), catalyst (50 mg) and toluene (15 mL) were put in a 50 mL two-necked round bottom flask. The flask with the reaction mixture with a reflux condenser attached was immersed in a silicon oil bath preheated to the reaction temperature. The reaction mixture was refluxed under vigorous stirring (700 rpm) for the required time under air flow. After reaction, the mixture was cooled, the catalyst was removed by filtration, and GC–MS was used to analyze the filtrate. The conversions were determined based on concentration of alcohols. The selectivities were calculated based on aldehydes or ketones as the only products. Most reactions were repeated at least three times and the average values of conversions were used.

2.3.2. 1,3,5-Trimethylbenzene oxidation

In a typical oxidation reaction, 1,3,5-trimethylbenzene (required amount in mL) and catalyst (100 mg) were put in a 50 mL two-necked round bottom flask. The flask with the reaction mixture with a reflux condenser attached was immersed in a silicon oil bath pretreated at 130 °C. The reaction mixture was then heated at 130 °C under vigorous stirring (700 rpm) for a certain time under air flow. After reaction, the mixture was cooled, the catalyst was removed by filtration, and GC–MS was used to analyze the filtrate. The conversions were determined based on concentration of substrates. The selectivities were calculated based on aldehydes, acids and esters as the products.

3. Results

3.1. Structural characterization of cation promoted mesoporous manganese oxides

Fig. 1A and B represents the low and the wide angle PXRD patterns of the UCT-18 materials, respectively. The low angle diffraction lines, like those of other UCT materials, indicate the existence of an ordered mesostructure. The low-angle PXRD line positions are almost the same for UCT-18 and UCT-1 materials (in nm) indicating very similar particle sizes (Table 1). According to the model of UCT materials, the low angle diffraction line positions correspond to the average nanoparticle size. The wide-angle PXRD patterns suggest an amorphous nature of the materials. The wide-angle PXRD patterns of UCT-18-Cs at different calcinations temperatures are shown in Fig. S1. The material is amorphous at low calcination temperatures (<450 °C) and transforms to crystalline bixbyite phase (Mn₂O₃) at elevated temperatures (>450 °C). The N₂ adsorption and desorption isotherms (Fig. 1C), show Type IV adsorption isotherms, followed by a Type I hysteresis loop, indicating regular mesoporous structures for all materials. The BET surface areas are summarized in Table 1. All the UCT-18 materials exhibit higher surface areas with UCT-18-Na having the maximum (152 m² g⁻¹). The BJH desorption pore size distributions of UCT-18 materials are the same (pore diameter 3.4 nm) (Fig. 1D, Table 1). The unique features of UCT materials are the expansion of d spacings and pore sizes upon heat treatment, which is the opposite of conventional mesoporous materials, where mesopores shrink upon heat treatment [35]. The cation promoted UCT-18-Cs material shows a similar increase of pore size distributions with rising calcination temperatures. The pore size increased from 3.4 nm (250 °C) to 7.8 nm (550 °C) (Table S1, Fig. S2). The FE-SEM images of UCT-18 materials (Fig. 2A–E) show very similar features with no distinguishable differences. They all show aggregated micron size rounded particles. The HR-TEM images (Fig. 2F–H) show aggregated nanoparticles with an average particle size of 10–12 nm and formation of a porous network in between the particles. The higher magnification HR-TEM images (Fig. 2B) indicate that the nanoparticles are crystalline. The lattice fringes of 0.49 nm and 0.27 nm can be indexed to the crystal phase (200) and (222) of the Mn₂O₃ (bixbyite). The lack of diffraction in the PXRD can be attributed to the nano-particle nature of the materials. The Mn/Cs (mol/mol) ratio for UCT-18-Cs was found to be 3000/1 by ICP-MS, which is quite different from the nominal ratio (Mn/Cs, 100/1, mol/mol), probably excess ions were eliminated by washing.

The relative basicity of the materials was determined by CO₂ chemisorption studies, because of the known role of basicity in oxidation reactions. The CO₂ adsorption isotherms at 298 K (Fig. 3) indicate an increase in basicity with addition of alkali metal ions for the manganese oxide resulting in an increase of the adsorbed volume of CO₂ being higher for promoted samples. The differences in the adsorbed CO₂ volume are more prominent when the temperature of CO₂ adsorption was decreased from 298 K to 198 K. (Fig. S3). The initial CO₂ uptake (slope) is higher for the promoted samples (UCT-18) suggesting a stronger interaction

Table 1
Structural parameters of UCT-1 and UCT-18^a.

Metal	Title	Surface area (m ² g ⁻¹)	BJH desorption pore diameter (nm)	Pore volume (cm ³ g ⁻¹)	Low-angle PXRD peak position (nm)
Mn	UCT-1	200	2.8	0.153	6.7
Mn/Cs	UCT-18-Cs	78	3.4	0.107	7.6
Mn/Na	UCT-18-Na	152	3.4	0.192	8.5
Mn/K	UCT-18-K	149	3.4	0.161	8.5
Mn/Ca	UCT-18-Ca	101	3.4	0.163	7.1
Mn/Mg	UCT-18-Mg	97	3.4	0.151	8.9

^a All materials were calcined at 150 °C for 12 h, then at 250 °C for 3 h.

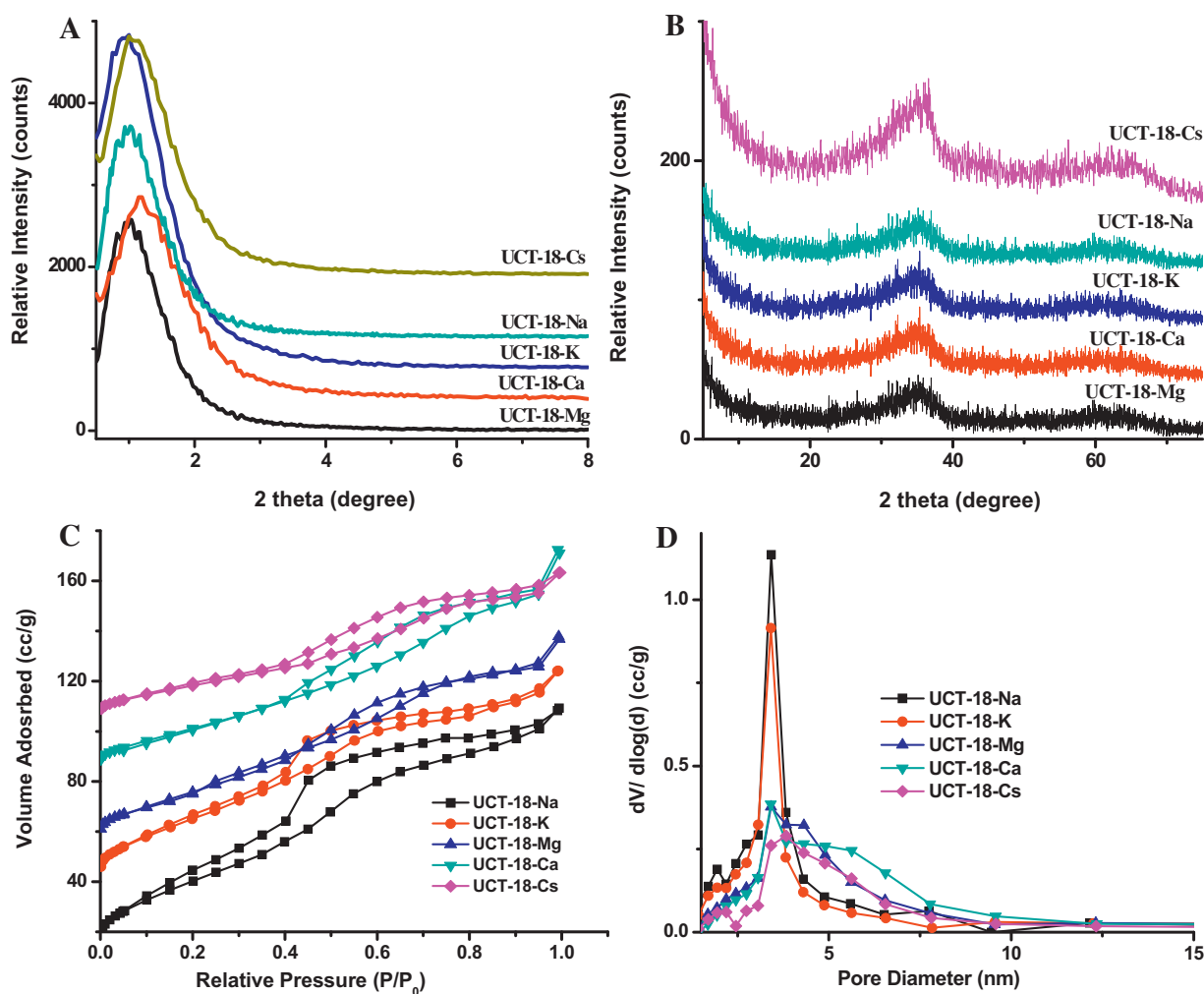


Fig. 1. (A) Low angle (0.5°–8°) PXRD patterns, (B) wide angle (5°–75°) PXRD patterns, (C) N₂ sorption isotherms, and (D) BJH desorption pore size distributions of cation promoted mesoporous manganese oxides (UCT-18-X, X = Mg²⁺, Ca²⁺, K⁺, Na⁺, and Cs⁺).

(chemisorption) between adsorbent and adsorbate (CO₂). At all temperatures, the UCT-18-Cs material is more basic in nature compared to UCT-1, K-OMS-2 and nonporous commercial Mn₂O₃.

The structural stabilities of UCT-1 and UCT-18-Cs materials were investigated in a temperature range of 250 °C to 550 °C in air by TR-PXRD (Fig. 4A and B). The samples are amorphous, without any crystalline long-range order. Both UCT-1 and UCT-18-Cs materials transform to the bixbyite (Mn₂O₃) phase with rising temperatures. Interestingly, the addition of trace amounts of Cs cations (Mn/Cs, 3000/1) has a marked effect on the crystallization temperature. The non-promoted mesoporous manganese oxide (UCT-1) transform from an amorphous state to a crystalline state around 350 °C, whereas UCT-18-Cs can retain the amorphous state up to 400 °C before crystallizing directly to the bixbyite (Mn₂O₃) phase. The oxidation reduction profiles of the materials were tested by the temperature programmed reduction (H₂-TPR) and oxidation (O₂-TPO) studies. The two major reduction peaks in the H₂-TPR profile (Fig. 5A) indicate a two-step reduction (Mn₂O₃ to Mn₃O₄ and Mn₃O₄ to MnO) [37]. When Cs⁺ is incorporated in the manganese oxide (UCT-18-Cs), clear shifts of reduction temperatures to lower values (280 °C, 420 °C in UCT-1 and 260 °C, 400 °C in UCT-18-Cs) were observed, which indicate the easy reducible nature of UCT-18-Cs. Whereas, opposite to that of the reduction profile, the oxidation peak shifted to a higher temperature for the UCT-18-Cs (483 °C) with respect to nonpromoted UCT-1 (477 °C) in

the O₂-TPO profile (Fig. 5B). The temperature programmed desorption (O₂-TPD) under Ar was performed to look into the surface oxygen activity of the materials in the oxidation reaction. A major O₂ loss from both of the materials was observed (532 °C for UCT-1 and 570 °C for UCT-18-Cs) in the O₂-TPD (Fig. 5C), which can be ascribed to the loss of lattice oxygen near the surface of the material [38].

The XPS measurements were done to investigate the oxidation states of manganese and binding energies of different elements in the materials. The XPS results show that the binding energies (BEs) of Mn fall in the region of BEs of Mn³⁺ for all the materials with negligible differences [39] (Table S2, Fig. S4) which is in good agreement with the Mn₂O₃ phase by both H₂-TPR and PXRD analyses. The O 1s region was deconvoluted to three components corresponding to three different oxygen species with distinct binding environments. The first component O_s is the structural or lattice oxygen. The deconvolution results suggest that the area of the O_s peak in all the promoted UCT-18 materials have a relatively higher ratio (Table S2) than that in the nonpromoted UCT-1 material.

3.2. Catalytic reactions

3.2.1. Oxidation of benzyl alcohol

The oxidation of benzyl alcohol was selected as a model reaction to evaluate the catalytic performances of ion promoted mesoporous

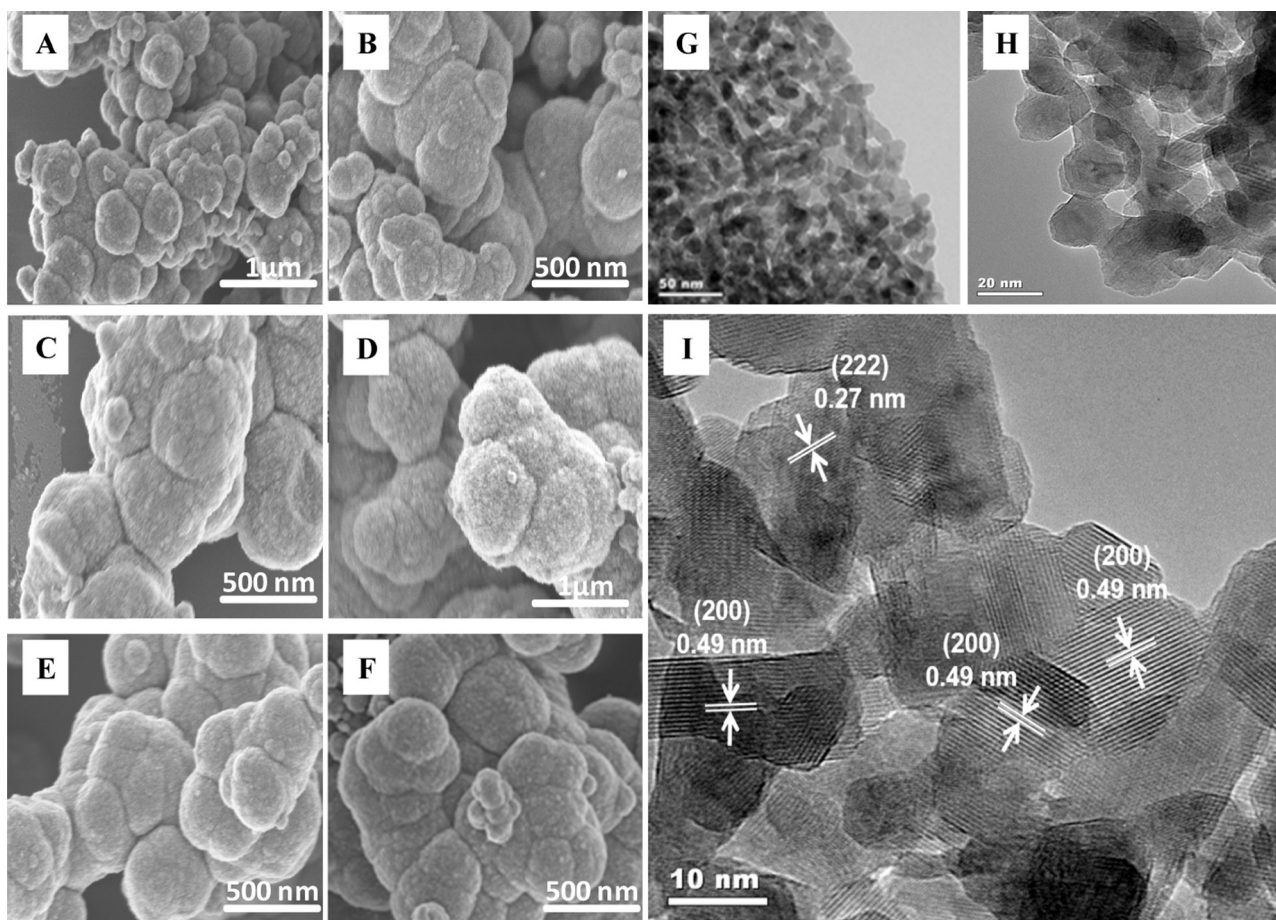


Fig. 2. FE-SEM images of (A) UCT-18-Cs, (B) UCT-18-Na, (C) UCT-18-K, (D) UCT-18-Ca, (E) UCT-18-Mg (F) UCT-1 materials and HR-TEM images of UCT-18-Cs material (G, H) at lower magnifications (I) at higher magnification. The measured lattice distances 0.49 and 0.27 nm are indexed to bixbyite Mn_2O_3 (200) and (222) planes.

manganese oxides. Fig. 6A shows the catalytic activity of K^+ promoted mesoporous manganese oxide (UCT-18-K), nonpromoted UCT-1 and K-OMS-2 (one of K^+ promoted state-of-the-art manganese oxide catalysts effective for aerobic alcohol oxidation [40]) under identical conditions. The promoted UCT-18-K exhibit higher conversion of benzyl alcohols compared to UCT-1, K-OMS-2 and K-OMS-2 calcined at 150°C for 12 h + 250°C for 3 h. The conversion

was 100% at 110°C for UCT-18-K. The selectivity in all cases was 100%, as benzaldehyde was the only product observed by GC–MS. To investigate the leaching of ions in solution, the catalyst was removed after the reaction by filtration. The filtrate was tested by AAS, no K or Mn ions were found in the filtrate.

3.2.2. Catalyst screening

The cation amount of the materials and the corresponding catalytic activity were also tested. Apart from the nominal Mn/cation (100/1, mol/mol) ratio, the UCT-18-K was also synthesized with different Mn/K molar ratios (50/1, 20/1 and 10/1). The Mn/K molar ratio 10/1 did not give any clear reaction gel, as the surfactant became insoluble and precipitated. The benzyl alcohol oxidation was done by UCT-18-K with different Mn/K molar ratios (Fig. S5). The Mn/K molar ratio 100/1 was found to be optimal. After demonstrating the superior catalytic activity of K^+ promoted manganese oxide (UCT-18-K) over nonpromoted and other K^+ promoted manganese oxide (UCT-1, K-OMS-2), other promoted oxides with different alkali metal cations (UCT-18-Mg, UCT-18-Ca, UCT-18-Na, UCT-18-Cs) were prepared. Selective aerobic oxidation of structurally different alcohols was performed to evaluate the catalytic performance of mesoporous UCT-1 and UCT-18 materials. Fig. 6B describes the increase of activity with the addition of metal ions for 4 different alcohols. There is a trend of increasing activity observed in the following order $\text{UCT-1} < \text{UCT-18-Mg} < \text{UCT-18-Ca} < \text{UCT-18-K} < \text{UCT-18-Na} < \text{UCT-18-Cs}$. This trend in activity is related to both the size and charge of the ions in manganese oxide (higher ratio resulted in higher catalytic activity). The observed trend suggests

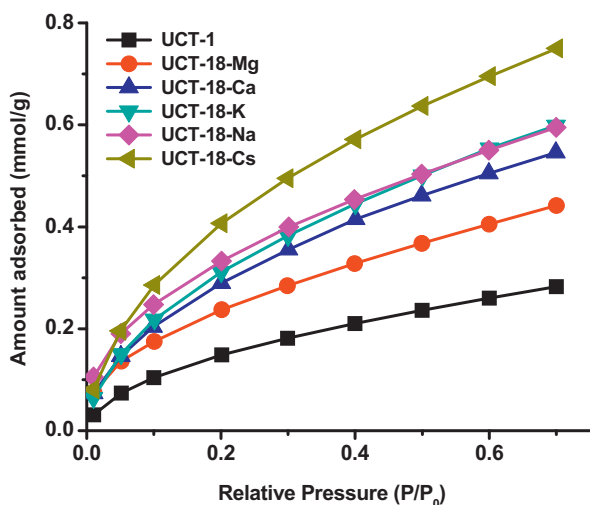


Fig. 3. CO_2 adsorption isotherms of UCT-1 and UCT-18-X, $\text{X} = \text{Mg}^{2+}$, Ca^{2+} , K^+ , Na^+ , and Cs^+ at 298 K.

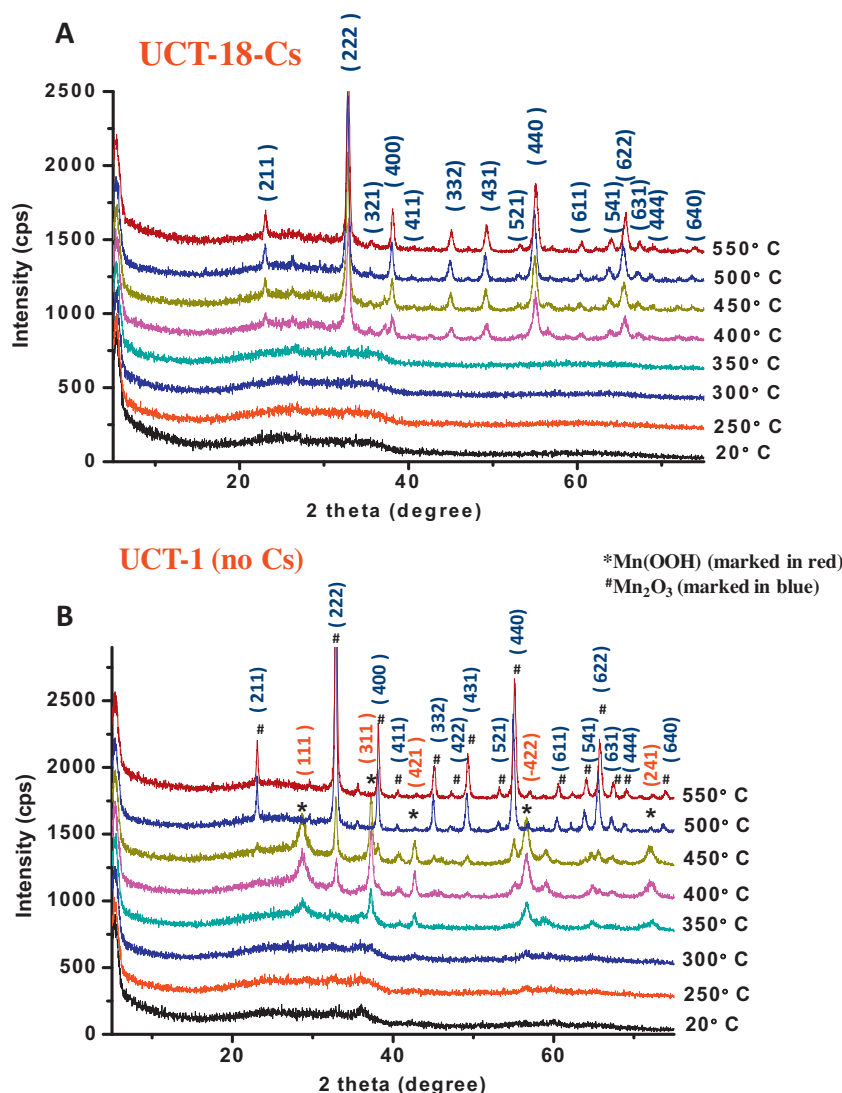


Fig. 4. Temperature resolved in situ PXRD (TR-PXRD) of (A) UCT-18-Cs, and (B) UCT-1. The materials were ramped at $5^{\circ}\text{C min}^{-1}$ up to 550°C . The diffraction patterns were obtained in the range of $5\text{--}75^{\circ} 2\theta$ at a scanning rate of $2^{\circ} \text{ min}^{-1}$.

that the promoted materials are always better than nonpromoted ones and Cs is the best promoter in the reaction.

3.2.3. Oxidation of various alcohols

The UCT-18-Cs (as the most active promoted UCT-18) and non-promoted UCT-1 were selected for the further testing of oxidations of structurally different alcohols. Table 2 summarizes the oxidation of 12 different alcohols catalyzed by the UCT-18-Cs and UCT-1. The UCT-18-Cs catalyst showed significantly higher activity for the conversion of all the alcohols to aldehydes or ketones as compared to UCT-1. UCT-18-Cs oxidized various types of structurally different alcohols with almost 100% conversions.

UCT-18-Cs was capable of oxidizing aromatic [Entry 1–11, Table 2], aliphatic [Entry 12, Table 2], primary [Entry 1–8, Table 2] and secondary [Entry 9, Table 2] alcohols selectively into the corresponding carbonyl compounds. For long chain aliphatic alcohol [Entry 12, Table 2] the conversion was less and a longer reaction time was required. The alcohols containing S and N as heteroatoms [Entry 7, 8, Table 2] were converted to the corresponding aldehydes selectively. In the case of oxidation of piperonyl alcohol [Entry 6, Table 2] to piperonyl aldehyde, the UCT-18-Cs had ten times better conversion than UCT-1. The UCT-18-Cs converted 1,3-Benzenedimethanol chemoselectively (92%

selectivity) to monoaldehyde with 93% conversion [Entry 11, Table 2].

3.2.4. The effect of air and solvent, calcination temperatures and comparison with conventional catalysts

The selective oxidation of alcohols was performed under air, which is considered to be a mild oxidant. In order to investigate the role of air as an oxidant, a model reaction (benzyl alcohol oxidation) was performed under N_2 . The conversion decreased significantly (30% at 85°C) compared to that of the reaction done under air (>99% at 85°C). A significant decrease of conversion (10% at 85°C , 100% selectivity) was observed again, when acetonitrile was used as solvent instead of toluene. To evaluate the reusability, the UCT-18-Cs catalyst was removed by filtration, washed with reaction solvent (toluene) and excess ethanol, dried under vacuum and reactivated at 250°C for 2 h prior to each catalytic cycle. The UCT-18-Cs exhibited only a slight catalytic activity loss compared to the fresh catalyst (>99% conversion, 100% selectivity) even after the 4th reuse (90% conversion, 100% selectivity) (Fig. 7A). To study the effect of pore size, a model reaction (benzyl alcohol oxidation) was performed using UCT-18-Cs and UCT-1 calcined at different temperatures (Fig. 7B). The UCT-18-Cs was more active than UCT-1 despite the overall decrease of activity with rising calcination

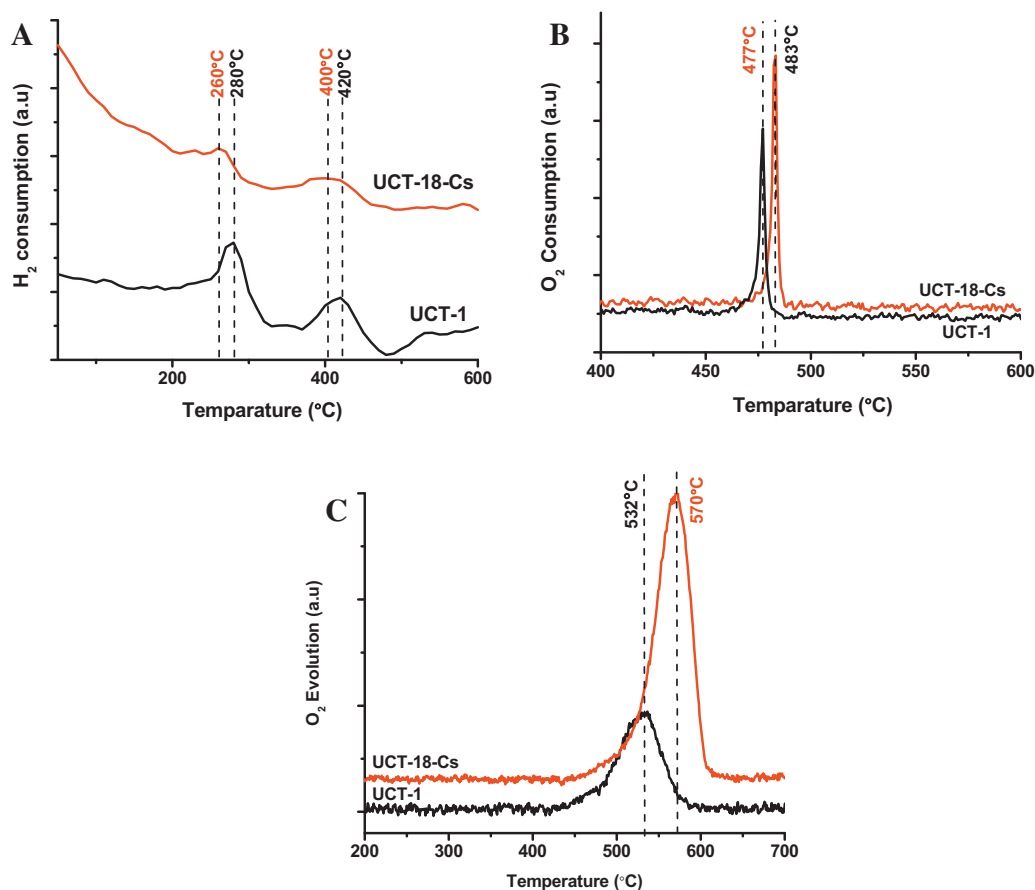


Fig. 5. (A) H_2 -TPR and (B) O_2 -TPO and (C) O_2 -TPD profile of UCT-18-Cs and UCT-1. The measurements were conducted from room temperature to 700°C ($10^\circ\text{C min}^{-1}$) under a stream of 10% H_2/Ar for H_2 -TPR, 10% O_2/Ar for O_2 -TPO and pure Ar for O_2 -TPD with a flow rate of 50 sccm.

temperatures. Kinetic experiments were performed for oxidation of benzyl alcohol at 85°C with UCT-18-Cs. A first order dependence of the alcohol concentration on rate was observed from the liner relationship of $\ln [\text{alcohol}]$ vs time with a rate constant of 0.026 min^{-1} (Fig. S6). Commercial Mn_2O_3 and K-OMS-2 were also tested for oxidation of 1-decanol for comparison (Table S3). The UCT-18-Cs material was found to be much more active (30% conversion) than UCT-1 (3% conversion), nonporous commercial Mn_2O_3 (0% conversion) and K-OMS-2 (15% conversion). The conversions for UCT-18-Cs were very high and selective to the carbonyl with no over-oxidation (to carboxylic acid).

3.2.5. The oxidation of 1,3,5-trimethylbenzene (C–H activation)

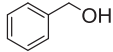
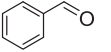
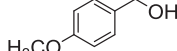
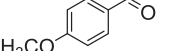
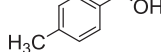
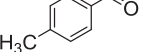
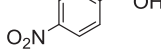
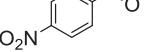
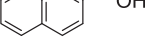
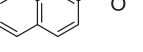
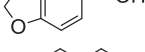
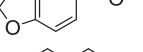
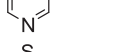
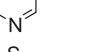
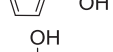
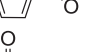
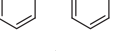
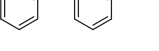


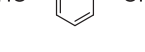
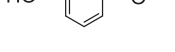


The UCT-18-Cs was investigated further for the activation of relatively inert C–H bond. 1,3,5-trimethylbenzene (mesitylene) was used as substrate. The UCT-18-Cs catalyst successfully oxidized 1,3,5-trimethylbenzene (10 mL) to 3,5-dimethylbenzoic acid with a very high conversion (99%) and selectivity (90%) under aerobic and solvent free conditions (Table 3). Once again, the UCT-18-Cs (99% conversion) demonstrated enhanced catalytic performance over UCT-1 (52% conversion) [Entry 4, Table 3] under similar conditions. The UCT-18-Cs also exhibited a high conversions (95%) and selectivity ($\sim 90\%$) with different scale of reactants (5 mL, 25 mL) [Entry 2–3, Table 3]. The oxidation of 1,3,5-trimethylbenzene also produced (3,5-dimethylphenyl)methyl ester ($\sim 10\%$ selectivity) via cross dehydrogenative coupling. The oxidation was also conducted with different catalyst amounts (Table S4). Using 100 mg catalyst gave the highest conversion and selectivity, while the lower catalyst loading (25 mg, 50 mg) gave larger amounts of 3,5-dimethylbenzyl alcohols and 3,5-dimethylbenzaldehyde side products along with

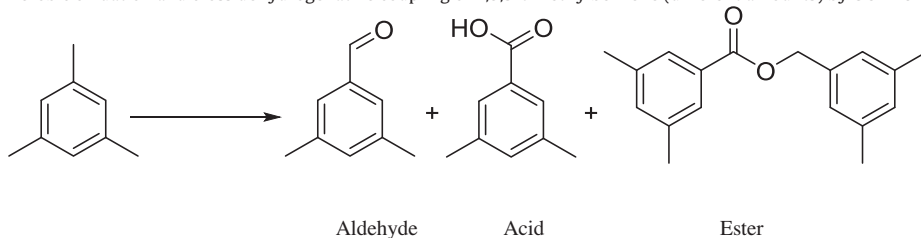
acid and ester. These results give valuable information about the intermediates in the oxidation of 1,3,5-trimethylbenzene. The reaction is initiated by the formation of alcohols followed by oxidation to the aldehyde, acid and esters. Moreover, the oxidation of 1,2,4-trimethylbenzene produced two different isomeric acids and three different isomeric benzylic esters with a very high conversion (94%) and selectivity (60/30, acids/esters) (Table S5).

4. Discussion

In this work, alkali ion promoted mesoporous manganese oxide catalysts (UCT-18, University of Connecticut mesoporous materials) were designed for liquid phase oxidation reactions. In the synthesis of UCT-18, Mn precursors along with the other ionic sources were confined in inverse surfactant (P123) micelles, which were then packed to form mesoporous materials. The uncontrolled aggregation of oxo-clusters was prevented by surfactant molecules in the reverse micelles and the interface modifier (1-Butanol). The hydrotropic nitrate ion increased the solubility of the surfactants by decreasing the aggregation number. The nitrate ions penetrated into the micelles to hydrate it and pulled the positively charged oxo clusters into the micelles [41]. The reaction was driven by evaporation of the solvent at 120°C and thermal NO_x formation (from the nitrate ion) to control the sol-gel chemistry of Mn sols. The surfactants in the resulting materials were washed off with ethanol (solvent extraction). The mesopores were formed by connected inter-particle voids. The chemisorbed nitric oxides and carboxylates were removed from the structure by heating the material at 150°C for 12 h and 250°C for 3 h under air [35].

Table 2Aerobic selective oxidation of different alcohols by UCT-1 and UCT-18-Cs.^a

Entry	Substrate	Product	Time (h)	Catalyst	Conversion ^{b,c} (%)
1			2 ^d	UCT 1 UCT-18-Cs	24 >99
2			2 ^d	UCT 1 UCT-18-Cs	12 >99
3			2 ^d	UCT 1 UCT-18-Cs	30 >99
4			2	UCT 1 UCT-18-Cs	85 >99
5			2	UCT 1 UCT-18-Cs	45 >99
6			4	UCT 1 UCT-18-Cs	10 >99
7			2	UCT 1 UCT-18-Cs	40 95
8			2	UCT 1 UCT-18-Cs	70 92
9			2	UCT 1 UCT-18-Cs	30 >99
10			15	UCT 1 UCT-18-Cs	8 50
11			6	UCT 1 UCT-18-Cs ^e	80 93
12			15	UCT 1 UCT-18-Cs	3 30

^a Reaction conditions: alcohols (1.0 mmol), toluene (15 mL), catalyst (50 mg), 110 °C, under air flow.^b Conversion (%) of alcohols = $[1 - (\text{concentration of alcohols after reaction}) \times (\text{concentration of alcohols before reaction})^{-1}] \times 100$.^c Selectivity was 100%, no products other than aldehyde and ketone were found.^d Reactions were performed at 85 °C.^e Selectivity was 92%, the other product was di-aldehyde for UCT-18-Cs.**Table 3**Aerobic oxidation and cross dehydrogenative coupling of 1,3,5-trimethylbenzene (different amounts) by UCT-18-Cs^a

Entry	Catalyst	Amount (mL)	Time (h)	Conversion ^b (%)	Selectivity ^c (%)		
					Aldehyde	Acid	Ester
1	UCT-18-Cs	5 (35 mmol)	36	95	nd	88	12
2	UCT-18-Cs	10 (70 mmol)	40	99	1	90	9
3	UCT-18-Cs	25 (175 mmol)	72	91	nd	91	9
4	UCT-1	10 (70 mmol)	40	52	7	69	24

^a Reaction conditions: 1,3,5-trimethylbenzene (required amount in mL), catalyst (100 mg), 130 °C, air flow.^b Conversion (%) of 1,3,5-trimethylbenzene = $[1 - (\text{concentration of 1,3,5-trimethylbenzene after reaction}) \times (\text{concentration of 1,3,5-trimethylbenzene before reaction})^{-1}] \times 100$.^c Selectivity (%) of product = $[(\text{concentration of product}) \times (\text{total concentration of all products})^{-1}] \times 100$. nd = not detected (<1%). The Entries signify the high catalytic performance of the catalyst in different scale of the reactant (1,3,5-trimethylbenzene).

Despite the promoter ions being mentioned several times in the literature, their major role in catalytic reactions is still unclear [42–45]. A trend of increasing catalytic activity with the increasing size/charge ratio of promoter cations has not been previously

observed. One possible explanation concerning the role of promoter ions in the enhanced catalytic activity is the alteration of the surface basicity. Alkali metal ions on the surface of the oxides are known to increase the basicity of the material due to their

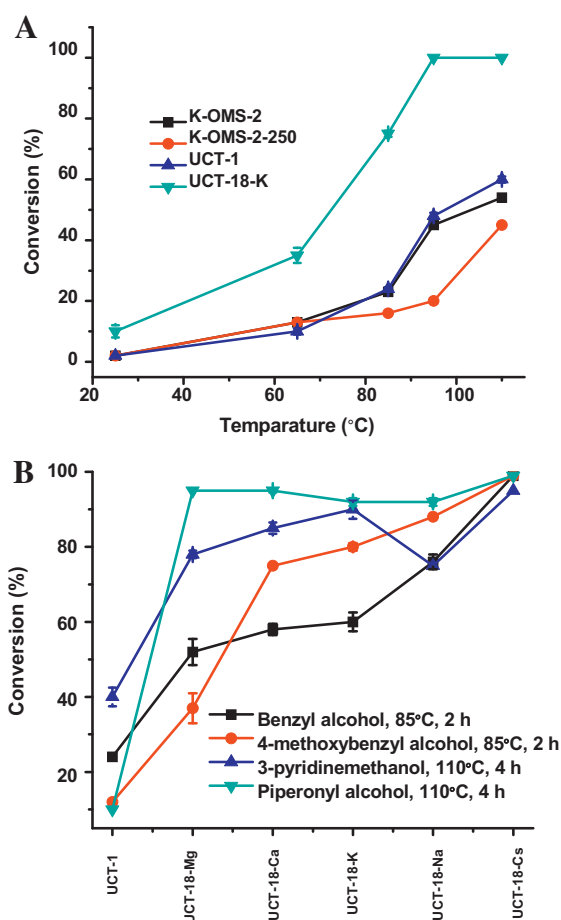


Fig. 6. (A) The comparison of activity in benzyl alcohol oxidation at different temperatures. Reaction conditions: benzyl alcohol (1.0 mmol), catalyst (50 mg), toluene (15 mL), under air flow, 2 h. (B) The oxidation of alcohols by UCT-1 and UCT-18. Reaction Conditions: alcohols (1.0 mmol), toluene (15 mL), catalyst (50 mg), under air flow, 85°C/110°C, 2 h/4 h.

electropositive nature [46]. The basic sites can be considered either as defects in the material or as enhanced electron density of the framework oxygen due to the presence of electropositive cations [47]. The effect of surface Cs causes the binding energy of lattice oxygen to decrease in energy as discussed by Santos et al., which also correlates with the increase of surface basicity [7]. The presence of basic sites on the manganese oxide materials promote the dehydration step by aiding the deprotonation of the alcohol, which is an important step for partial oxidation [48]. The basicity of the materials also promotes the oxidation of alkylbenzenes [49]. Therefore, increasing the basicity of mesoporous manganese oxide by incorporating alkali metal ions can enhance the catalytic activity for oxidation and esterification. In this work trace amounts of alkali metal ions (Mn/ion, >1000/1) were incorporated in the manganese oxide materials. However, the ions caused a remarkable increase in the catalytic activity towards oxidative transformations.

The relative basicities of materials were evaluated by CO₂ chemisorption experiments (Fig. 3). There is a trend of increasing basicity for the promoted materials, which correlates with the size/charge ratio of the cations. Like the trend observed for the oxidation of different alcohols (Fig. 6B), a similar trend was observed for the basicity of the materials, with Cs promoted material being the most basic. The UCT-18-Cs also exhibited higher basicity than nonpromoted UCT-1, other active promoted manganese oxides (K-OMS-2), and commercial nonporous Mn₂O₃ at different temperatures. Therefore, the basicity of the promoted materials plays

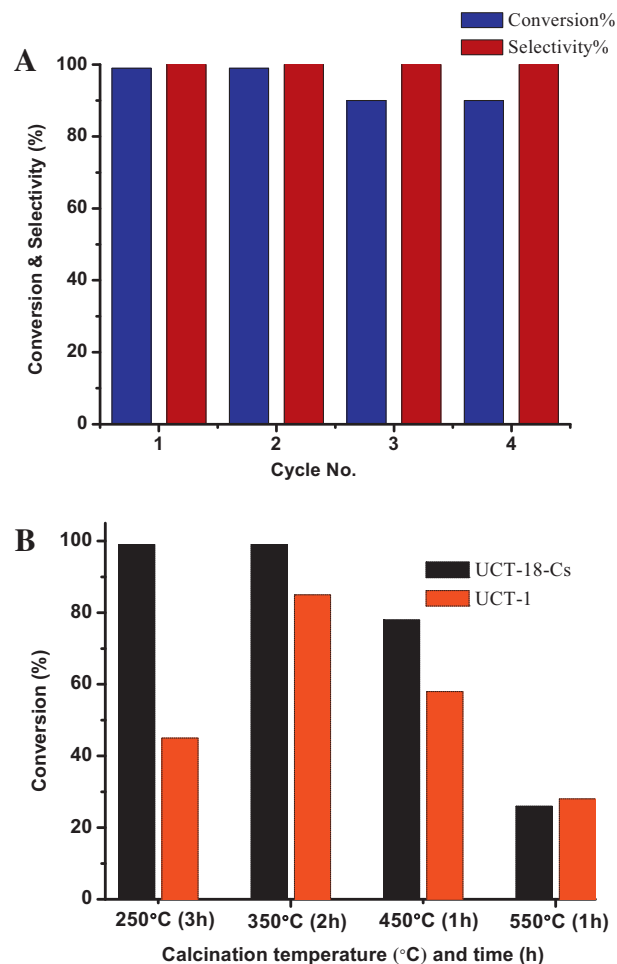


Fig. 7. (A) Reusability of UCT-18-Cs in benzyl alcohol oxidation. Reaction conditions: benzyl alcohol (1.0 mmol), UCT-18-Cs (50 mg), toluene (15 mL), 85°C, under air flow, 2 h. (B) Effect of Calcination temperature on UCT-1 and UCT-18-Cs in alcohol oxidation. Reaction conditions: benzyl alcohol (1.0 mmol), UCT-18-Cs (50 mg), toluene (15 mL), 110°C, under air flow, 2 h.

an important role in the higher activity in oxidation of alcohols and alkylbenzenes. Despite the fact that adding base in the reaction can increase the activity in oxidation in many systems, an efficient oxidation process should not involve any additives such as base or acid [50]. The bifunctional nature (redox and basic) of UCT-18-Cs can enhance the oxidation activity without any additional base. The results from Table S6 show that adding base in the system with the nonpromoted material (UCT-1) did not form acid or ester products. Therefore, the bifunctional nature is believed to be playing a role in both oxidation of 1-decanol to 1-decanoic acid and esterification of 1-decanoic acid and 1-decanol.

The UCT-18-Cs material shows an increase of pore size with rising calcination temperatures (Table S1, Fig. S2) due to the increase of nanoparticle size and intra particle voids (mesopores). Smaller particle sizes and higher surface areas provide more surface defects, which in turn act as active sites [51,52]. Hence the decrease of surface area with heat treatment can be the reason behind the reduction of catalytic activity (Fig. 7B). The UCT-18-Cs is also found to be more active in the amorphous state than in the pure crystalline state, despite exhibiting higher activity than UCT-1 for all different states of the materials. The TR-PXRD (Fig. 4) data indicate that the amorphous state is more stable for UCT-18-Cs than UCT-1 with heat treatment. The higher catalytic activity of promoted UCT-18-Cs compared to nonpromoted UCT-1 can also be attributed to the retention of the amorphous state. Manganese oxides in the

amorphous states are known to be more active than in crystalline states [13,14,53]. The labile lattice oxygen of manganese oxide is one of the reasons for enhanced catalytic activity of amorphous manganese oxides [54]. The lack of crystallinity in the amorphous state of the materials promotes a more available supply of lattice oxygen. The smaller particle sizes and higher surface areas of the amorphous materials are other contributing factors.

The activity of the manganese oxides can be linked to the ease of reducibility of the materials. The low reduction temperatures of promoted UCT-18-Cs (280 °C, 420 °C in UCT-1 and 260 °C, 400 °C in UCT-18-Cs), as observed in H₂-TPR studies (Fig. 5A) indicate an increase of mobility and accessibility of lattice oxygen. The presence of Cs⁺ induces a more facile supply of lattice oxygen, which can create defects in the materials [7]. The defects promote the adsorption of the substrate, and high adsorption capacity of the mesoporous materials is a well established property [55]. The effect on lattice oxygen was more prominently observed in the O₂-TPD studies (Fig. 5C). The UCT-1 and UCT-18-Cs evolve lattice oxygen at around 532 °C and 570 °C, respectively. Though these materials are amorphous in nature they still have some crystallinity with a framework structure as observed in HR-TEM images. So the term lattice (or bulk) oxygen can be used for the amorphous UCT-1 and UCT-18-Cs materials. The involvement of lattice oxygen in the catalytic activity suggests that the reaction goes through the Mars-Van-Krevelen mechanism [56–59]. The Mn³⁺ species disproportionates to Mn²⁺ and Mn⁴⁺ species under oxidative conditions [60]. The adsorbed alcohol molecules are oxidized with multi-electron transfer between the Mn centers (Scheme S1). The reduced Mn species however can get oxidized by labile lattice oxygen with creation of oxygen vacancies. The resulting oxygen vacancies are finally replenished by gas phase oxygen molecules. The presence of three different oxygen species in different binding environments was established by XPS studies (Table S2). The areas of O_s peaks (structural or lattice oxygen) in all the promoted UCT-18 materials are relatively higher than nonpromoted UCT-1. Therefore, the easily reducible best promoted UCT-18-Cs evolve labile lattice oxygen more readily by creating active sites, which is related to the enhanced catalytic activity.

Selective oxidation of several different alcohols were performed by nonpromoted (UCT-1) and promoted (UCT-18) mesoporous manganese oxides. The activity followed the series of cations according to the size/charge ratio, UCT-1 < UCT-18-Mg < UCT-18-Ca < UCT-18-K < UCT-18-Na < UCT-18-Cs. Among the promoted oxides, the Cs promoted one performed best. The Cs promoted material (UCT-18-Cs) was then used for oxidation of 12 different alcohols to corresponding aldehydes and ketones. The reaction exhibited very high conversion (> 99% in most cases) in most cases under mild aerobic conditions. Only in the case of big and inactive 1-decanol [Entry 12, Table 2] the conversion was less. This may be due to the limitation of molecular transportation in the mesopores of the catalyst or the inactivity of the long chain aliphatic alcohol. Transition metal oxide based catalysts are notorious for not being ideal types of heterogeneous catalysts for the selective oxidation of alcohols containing heteroatoms (i.e. S and N), because the strong coordination of the heteroatom with the metal center results in deactivation of the catalyst [61]. However, UCT-18-Cs successfully and selectively catalyzed the alcohols containing S and N as heteroatoms [Entry 7, 8, Table 2] to the corresponding aldehydes. Moreover the recovered catalyst (UCT-18-Cs) gave conversions similar to the fresh catalysts in the case of oxidation of 2-thiophenemethanol. The excellent selectivity in the oxidation reactions can be attributed to the observations that aldehydes and ketones are the only products with no over-oxidation to carboxylic acids occurring. The catalytic performance of UCT-18-Cs can be restored by washing with toluene and methanol followed by reactivation at 250 °C for 2 h in air. The reactivation is required to

remove adsorbed species from the surface of the catalyst. The first order dependence of rate on alcohol concentration is also an indication of the rate determining step, which could involve adsorption of alcohols or desorption of aldehydes from the active sites of the catalyst surface. The lower activity under N₂ (30% conversion) compared to air (>99% conversion) is attributed to adsorbed oxygen on the catalyst surface and labile lattice oxygen. These observations also indicate the role of air in the oxidation reaction, as the loss of lattice oxygen is replenished by the oxygen coming from air [59]. The significantly reduced conversion (10% in acetonitrile) in polar solvent may be due to competitive binding of the solvents to the active sites of the catalyst [59]. The reaction in acetonitrile (100% selectivity for benzaldehyde, no other products were detected) also rules out the formation of toluene due to non oxidative disproportionation reaction of benzyl alcohol [62,63] in the reaction condition. The oxidation of the solvent, toluene (without the substrate) was carried out under identical conditions by UCT-18-Cs to verify if benzaldehyde was formed as a result of oxidation of toluene. The trace amount of benzaldehyde (<1%) formed after 15 h of reaction indicates that UCT-18-Cs selectively catalyzed the oxidation of alcohols in the mentioned reaction conditions. The oxidation of aromatic C–H bond required prolonged reaction time with a greater amount of catalyst. The relative activity of UCT-18-Cs to inactivated compounds is quite notable. For example, the oxidation of the inactivated long chain alcohol 1-decanol to 1-decanal shows a performance of UCT-18-Cs being better than nonpromoted UCT-1, K-OMS-2 (Table S3). Moreover, UCT-18-Cs can undergo solvent free green oxidation of inert 1,3,5-trimethylbenzene to 3,5-dimethylbenzoic acid with very high conversion (>90% conversion) and selectivity (90/10, acid/ester). This kind of green oxidation under mild and aerobic conditions has not been observed before. Even in the case of large scale transformation, the catalyst exhibited similar conversions and selectivities, (Table 3). The reaction also yielded (3,5-dimethylphenyl)methyl ester along with the acid. Formation of the ester is due to cross dehydrogenative coupling (CDC) of 1,3,5-trimethylbenzene or any other intermediates like corresponding alcohols, aldehydes or acids. Typical catalysts used for the cross dehydrogenative coupling contain metal centers like Ru, Rh, V, Cu with basic additives and TBHP as the oxidant [64–67]. The bifunctional nature of UCT-18-Cs (redox and basic) can promote the formation of esters under ambient aerobic and green conditions without the presence of base or expensive oxidants.

5. Conclusion

To summarize, the incorporation of trace amounts (Mn/ion, >1000/1) of alkali metal ions leads us to promoted mesoporous manganese oxides. The cation promoted materials (UCT-18) exhibited regular mesoporosity with pore sizes of 3.4 nm. These catalysts demonstrated other characteristic features of UCT materials (one low angle diffraction line, Type IV isotherm, aggregation of rounded micron size nanoparticles). The cation promoted mesoporous manganese oxides exhibited high catalytic performance for oxidation of alcohols to carbonyl compounds under mild aerobic reaction conditions in the following order UCT-1 < UCT-18-Mg < UCT-18-Ca < UCT-18-K < UCT-18-Na < UCT-18-Cs. The order followed the size/charge ratios of the incorporated cations, which correlates with the increase of relative basicity of the materials. The Cs promoted mesoporous manganese oxide was found to be the most active for selective alcohol oxidation reactions (>95% conversion in most cases, 100% selectivity). The UCT-18-Cs material demonstrated superior catalytic activity in the solvent free green oxidation of 1,3,5-trimethylbenzene to 3,5-dimethylbenzoic acid and (3,5-dimethylphenyl)methyl ester with very high conversions (>90% conversion) and selectivity (90/9, acid/ester). Such scalable, green

and mild aerobic oxidation and cross dehydrogenative coupling of relatively inert C–H bonds was observed for the first time. The enhancement in catalytic activity can be correlated to the bifunctional (redox and basic) nature of the material, which in turn correlates with the promoting effect of ions in the mesoporous manganese oxides. The easily reducible nature with retention of the amorphous phase reflects the greater amount of accessible lattice or structural oxygen, which also contribute to the enhanced catalytic activity. The use of mild reaction conditions, (use of air as the oxidant, at ambient pressure), excellent reusability and high activity towards inactive compounds make the UCT-18 (especially UCT-18-Cs) materials a new class of environmentally friendly oxidation catalysts. The tunable pore size and crystallinity through simple heating cycles make the materials more ubiquitous and this opens a new avenue for the design and application of heterogeneous catalysts.

Acknowledgments

This work was supported by the U.S. Department of Energy, Office of Basic Energy Sciences, Division of Chemical, Biological, and Geological Sciences under grant DE-FGO2-86ER13622.A000. We also thank Christopher Perkins of the Center for Environmental Sciences and Engineering, University of Connecticut, Storrs for assistance on ICP-MS and Dr. Frank Galasso and David Kriz for helpful discussions.

Appendix A. Supplementary data

Supplementary data associated with this article can be found, in the online version, at <http://dx.doi.org/10.1016/j.apcatb.2014.10.055>.

References

- [1] C. Kresge, M. Leonowicz, W. Roth, J. Vartuli, *Nature* 359 (1992) 710–712.
- [2] A. Corma, *Chem. Rev.* 97 (1997) 2373–2420.
- [3] A. Taguchi, F. Schüth, *Microporous Mesoporous Mater.* 77 (2005) 1–45.
- [4] Y. Rao, D.M. Antonelli, *J. Mater. Chem.* 19 (2009) 1937–1944.
- [5] A.S. Poyraz, S. Biswas, H.C. Genuino, S. Dharmarathna, C.H. Kuo, S.L. Suib, *ChemCatChem* 5 (2013) 920–930.
- [6] A. Grirrane, A. Corma, H. García, *Science* 322 (2008) 1661–1664.
- [7] V. Santos, M. Pereira, J. Órfão, J. Figueiredo, *Appl. Catal., B: Environ.* 88 (2009) 550–556.
- [8] N. Patel, R. Fernandes, A. Miotello, *J. Catal.* 271 (2010) 315–324.
- [9] Z.-R. Tian, W. Tong, J.-Y. Wang, N.-G. Duan, V.V. Krishnan, S.L. Suib, *Science* 276 (1997) 926–930.
- [10] S.L. Suib, *J. Mater. Chem.* 18 (2008) 1623–1631.
- [11] S.L. Brock, N. Duan, Z.R. Tian, O. Giraldo, H. Zhou, S.L. Suib, *Chem. Mater.* 10 (1998) 2619–2628.
- [12] T. Oishi, K. Yamaguchi, N. Mizuno, *ACS Catal.* 1 (2011) 1351–1354.
- [13] J. Hu, K. Sun, D. He, B. Xu, *Chin. J. Catal.* 28 (2007) 1025–1027.
- [14] A. Iyer, J. Del-Pilar, C.K. King'ondou, E. Kissel, H.F. Garces, H. Huang, A.M. El-Sawy, P.K. Dutta, S.L. Suib, *J. Phys. Chem. C* 116 (2012) 6474–6483.
- [15] X. Li, J. Xu, F. Wang, J. Gao, L. Zhou, G. Yang, *Catal. Lett.* 108 (2006) 137–140.
- [16] Y. Su, L.-C. Wang, Y.-M. Liu, Y. Cao, H.-Y. He, K.-N. Fan, *Catal. Commun.* 8 (2007) 2181–2185.
- [17] K. Yamaguchi, H. Kobayashi, T. Oishi, N. Mizuno, *Angew. Chem.* 124 (2012) 559–562.
- [18] S.C. Kim, W.G. Shim, *Appl. Catal., B: Environ.* 98 (2010) 180–185.
- [19] E.K. Nyutu, C.-H. Chen, S. Sithambaram, V.M.B. Crisostomo, S.L. Suib, *J. Phys. Chem. C* 112 (2008) 6786–6793.
- [20] Y. Uozumi, Y. Yamada, *Chem. Rec.* 9 (2009) 51–65.
- [21] C.P. Vinod, K. Wilson, A.F. Lee, *J. Chem. Technol. Biotechnol.* 86 (2011) 161–171.
- [22] M.J. Schultz, M.S. Sigman, *Tetrahedron* 62 (2006) 8227–8241.
- [23] T. Mallat, A. Baiker, *Chem. Rev.* 104 (2004) 3037–3058.
- [24] S. Shylesh, V. Schünemann, W.R. Thiel, *Angew. Chem. Int. Ed.* 49 (2010) 3428–3459.
- [25] Y. Ishii, S. Sakaguchi, T. Iwahama, *Adv. Synth. Catal.* 343 (2001) 393–427.
- [26] A.E. Shilov, G.B. Shul'pin, *Chem. Rev.* 97 (1997) 2879–2932.
- [27] Y. Yoshino, Y. Hayashi, T. Iwahama, S. Sakaguchi, Y. Ishii, *J. Org. Chem.* 62 (1997) 6810–6813.
- [28] A.R. Dick, K.L. Hull, M.S. Sanford, *J. Am. Chem. Soc.* 126 (2004) 2300–2301.
- [29] A.V. Shijina, N.K. Renuka, *React. Kinet. Catal. Lett.* 94 (2008) 261–270.
- [30] J.-E. Bäckvall, *Modern Oxidation Methods*, 2nd ed, Wiley-VCH, Weinheim, 2011.
- [31] M.D. Nikalje, A. Sudalai, *Tetrahedron* 55 (1999) 5903–5908.
- [32] T. Das, K. Chaudhari, E. Nandan, A. Chandwadkar, A. Sudalai, T. Ravindranathan, S. Sivasanker, *Tetrahedron Lett.* 38 (1997) 3631–3634.
- [33] Y. Bonvin, E. Callens, I. Larrosa, D.A. Henderson, J. Oldham, A.J. Burton, A.G. Barrett, *Org. Lett.* 7 (2005) 4549–4552.
- [34] T.M.A. Shaikh, A. Sudalai, *Eur. J. Org. Chem.* 2008 (2008) 4877–4880.
- [35] A.S. Poyraz, C.-H. Kuo, S. Biswas, C.K. King'ondou, S.L. Suib, *Nat. Commun.* 4 (2013) 2952.
- [36] A.S. Poyraz, C.-H. Kuo, E. Kim, Y. Meng, M.S.I. Seraji, S.L. Suib, *Chem. Mater.* 26 (2014) 2803–2813.
- [37] E. Stobbe, B. De Boer, J. Geus, *Catal. Today* 47 (1999) 161–167.
- [38] H.C. Genuino, S. Dharmarathna, E.C. Njagi, M.C. Mei, S.L. Suib, *J. Phys. Chem. C* 116 (2012) 12066–12078.
- [39] M. Özacar, A.S. Poyraz, H.C. Genuino, C.-H. Kuo, Y. Meng, S.L. Suib, *Appl. Catal., A: Gen.* 462 (2013) 64–74.
- [40] Y.C. Son, V.D. Makwana, A.R. Howell, S.L. Suib, *Angew. Chem.* 113 (2001) 4410–4413.
- [41] A.S. Poyraz, O.M. Dag, *J. Phys. Chem. C* 113 (2009) 18596–18607.
- [42] M. Arai, S. Nishiyama, S. Tsuruya, M. Masai, *J. Chem. Soc., Faraday Trans.* 92 (1996) 2631–2636.
- [43] M. Genta, S. Nishiyama, S. Tsuruya, M. Masai, *J. Chem. Soc., Faraday Trans.* 92 (1996) 1267–1275.
- [44] Q. Tang, X. Huang, C. Wu, P. Zhao, Y. Chen, Y. Yang, *J. Mol. Catal. A: Chem.* 306 (2009) 48–53.
- [45] Y. Li, D. Nakashima, Y. Ichihashi, S. Nishiyama, S. Tsuruya, *Ind. Eng. Chem. Res.* 43 (2004) 6021–6026.
- [46] Z. Helwani, M. Othman, N. Aziz, J. Kim, W. Fernando, *Appl. Catal., A: Gen.* 363 (2009) 1–10.
- [47] G. Martra, R. Ocule, L. Marchese, G. Centi, S. Coluccia, *Catal. Today* 73 (2002) 83–93.
- [48] N. Zheng, G.D. Stucky, *Chem. Commun.* 37 (2007) 3862–3864.
- [49] S.K. Jana, P. Wu, T. Tatsumi, *J. Catal.* 240 (2006) 268–274.
- [50] A. Abad, P. Concepción, A. Corma, H. García, *Angew. Chem. Int. Ed.* 44 (2005) 4066–4069.
- [51] K. Yamamoto, T. Imaoka, W.-J. Chun, O. Enoki, H. Katoh, M. Takenaga, A. Sonoi, *Nat. Chem.* 1 (2009) 397–402.
- [52] S. Dharmarathna, C.K. King'ondou, W. Pedrick, L. Pahalagedara, S.L. Suib, *Chem. Mater.* 24 (2012) 705–712.
- [53] H. Cao, S.L. Suib, *J. Am. Chem. Soc.* 116 (1994) 5334–5342.
- [54] J. Chen, J.C. Lin, V. Purohit, M.B. Cutlip, S.L. Suib, *Catal. Today* 33 (1997) 205–214.
- [55] M. Climent, A. Velty, A. Corma, *Green Chem.* 4 (2002) 565–569.
- [56] V.D. Makwana, Y.-C. Son, A.R. Howell, S.L. Suib, *J. Catal.* 210 (2002) 46–52.
- [57] C. Doornkamp, V. Ponec, *J. Mol. Catal. A: Chem.* 162 (2000) 19–32.
- [58] A.S. Poyraz, W. Song, D. Kriz, C.-H. Kuo, M.S.I. Seraji, S.L. Suib, *ACS Appl. Mater. Interfaces* 6 (2014) 10986–10991.
- [59] S. Dharmarathna, C.K. King'ondou, L. Pahalagedara, C.-H. Kuo, Y. Zhang, S.L. Suib, *Appl. Catal., B: Environ.* 147 (2014) 124–131.
- [60] T. Takashima, K. Hashimoto, R. Nakamura, *J. Am. Chem. Soc.* 134 (2012) 1519–1527.
- [61] B. Karimi, J.H. Clark, V. Budarin, *Angew. Chem. Int. Ed.* 46 (2007) 7210–7213.
- [62] M. Sankar, E. Nowicka, R. Tiruvalam, Q. He, S.H. Taylor, C.J. Kiely, D. Bethell, D.W. Knight, G.J. Hutchings, *Chem. Eur. J.* 17 (2011) 6524–6532.
- [63] S. Meenakshisundaram, E. Nowicka, P.J. Miedziak, G.L. Brett, R.L. Jenkins, N. Dimitratos, S.H. Taylor, D.W. Knight, D. Bethell, G.J. Hutchings, *Faraday Discuss.* 145 (2010) 341–356.
- [64] G. Majji, S. Guin, A. Gogoi, S.K. Rout, B.K. Patel, *Chem. Commun.* 49 (2013) 3031–3033.
- [65] J. Zhang, G. Leitus, Y. Ben-David, D. Milstein, *J. Am. Chem. Soc.* 127 (2005) 10840–10841.
- [66] C. Liu, S. Tang, L. Zheng, D. Liu, H. Zhang, A. Lei, *Angew. Chem.* 124 (2012) 5760–5764.
- [67] S.K. Rout, S. Guin, K.K. Ghara, A. Banerjee, B.K. Patel, *Org. Lett.* 14 (2012) 3982–3985.